

Blue Stragglers as tracers of the dynamical state of two clusters in the Small Magellanic Cloud: NGC 339 and NGC 419

F. DRESBACH,¹ D. MASSARI,^{2,3} B. LANZONI,^{1,2} F. R. FERRARO,^{1,2} E. DALESSANDRO,² S. RASO,² A. BELLINI,⁴ AND M. LIBRALATO⁵

¹*Dept. of Physics and Astronomy, University of Bologna, Via Gobetti 93/2, Bologna, Italy*

²*INAF - Osservatorio di Astrofisica e Scienza dello Spazio di Bologna, Via Gobetti 93/3, I-40129 Bologna, Italy*

³*University of Groningen, Kapteyn Astronomical Institute, NL-9747 AD Groningen, The Netherlands*

⁴*Space Telescope Science Institute, 3700 San Martin Drive, Baltimore, MD 21218, USA*

⁵*AURA for the European Space Agency (ESA), ESA Office, Space Telescope Science Institute, 3700 San Martin Drive, Baltimore, MD 21218, USA*

ABSTRACT

The level of central segregation of Blue Straggler stars proved to be an excellent tracer of the dynamical evolution of old star clusters (the so-called “dynamical clock”), both in the Milky Way and in the Large Magellanic Cloud. The A^+ parameter, used to measure the Blue Stragglers degree of segregation, has in fact been found to strongly correlate with the parent cluster central relaxation time. Here we studied the Blue-Straggler population of two young stellar systems in the Small Magellanic Cloud, namely NGC 339 (which is 6 Gyr old) and NGC 419 (with an age of only 1.5 Gyr), in order to study their dynamical state. Thanks to multi-epoch, high angular resolution Hubble Space Telescope observations available for both clusters, we took advantage of the stellar proper motions measured in the regions of the two systems and we selected a population of likely cluster members, removing the strong contamination from Small Magellanic Cloud stars. This enabled us to study, with unprecedented accuracy, the radial distribution of Blue Stragglers in these two extragalactic clusters and to measure their dynamical age. As expected for such young clusters, we found that both systems are poorly evolved from the dynamical point of view, also fully confirming that the A^+ parameter is a sensitive “clock hand” even in the dynamically-young regime.

Keywords: star clusters: individual (NGC 339, NGC 419) - Blue Stragglers - techniques: photometric - proper motion

1. INTRODUCTION

Globular Clusters (GCs) are dynamically active systems, where the frequent gravitational interactions among stars can drastically alter the internal structure. The time-scale of a cluster dynamical evolution depends on a variety of its properties, both internal (total mass, density, fraction of binaries, etc.) and external (tidal interaction in the host galaxy, local density). Determining the evolutionary state of GCs is therefore a complex task. Dynamical interactions also lead to the formation of exotic objects like Blue Straggler stars (BSSs). These peculiar stars are located on the extension of the main sequence (MS), in a color-magnitude diagram (CMD), in the region that is hotter and bluer than the turn-off point (TO) (Sandage 1953, Ferraro et al. 1992, 1993, 1997). BSSs are thought to be the result of two mass-enhancement processes, either mass-transfer in binary

systems (McCrea 1964) or stellar mergers resulting from direct collisions (Hills & Day 1976). Since BSSs are more massive than the average (in Galactic GCs they have masses of $\sim 1.2 M_{\odot}$, while the average stellar mass is $\langle m \rangle \sim 0.3 M_{\odot}$; Shara et al. 1997, Fiorentino et al. 2014, Raso et al. 2019), their level of central segregation is an indicator of the host system dynamical age. This concept was for the first time demonstrated from the analysis of the BSS radial distribution (yielding to the definition of the so-called dynamical clock (Ferraro et al. 2012) and then further defined by using the A^+ parameter (Lanzoni et al. 2016, Ferraro et al. 2018). This parameter is defined (Alessandrini et al. 2016) as the area enclosed between the cumulative radial distribution of BSSs and that of a reference (and lighter) population. As such, its value increases as the dynamical evolution of the cluster proceeds and makes heavier

stars sink in more rapidly than the less massive ones (Alessandrini et al. 2016, Lanzoni et al. 2016). Indeed, this parameter shows a tight correlation with structural/dynamical parameters, such as central relaxation time and core radius, which trace the cluster dynamical ageing (Ferraro et al. 2018). The same correlations were then confirmed in a few old extra-Galactic clusters located in the Large Magellanic Cloud (Ferraro et al. 2019). However, this kind of analysis has not yet been made for young star clusters. To this end, the Small Magellanic Cloud (SMC) represents an ideal environment since it is populated by several young ($t < 2$ Gyr) and intermediate age clusters ($t = 3 - 7$ Gyr). In this paper we analyze the Blue Straggler population of two star clusters, NGC 339 and NGC 419, located in this galaxy and with an age of 6 Gyr and 1.5 Gyr, respectively (Glatt et al. 2009). The study of their BSS populations has been hindered by the large contamination from SMC field stars that occupy the same region of the CMD. Traditional statistical techniques used to decontaminate from non-cluster members (e.g. Cabrera-Ziri et al. 2016, Dalessandro et al. 2019) may not work on a star-by-star basis, and thus could artificially alter the spatial distribution of the decontaminated sample. For this reason, a kinematic decontamination acting on each individual star is required. Thanks to the availability of multi-epoch observations obtained for both clusters with the *Hubble Space Telescope* (*HST*), from which relative proper motions (PMs) of individual stars have been measured (Massari et al. 2021), we have performed a kinematic study aimed at selecting BSS members of each cluster. Our final goal is to determine the dynamical age of these clusters and verify whether the BSS population can act as a dynamical indicator even in these younger systems.

The paper is organised as follows. In Section 2 we present the dataset and the PM measurements. In Section 3 we describe the decontamination procedure and the cluster membership analysis. In Section 4 we study the BSS population, determining the A^+ parameter and the dynamical state of the clusters, and we discuss the results. The conclusions are provided in Section 5.

2. DATA ANALYSIS

The data available for the two clusters have been obtained from observations made with *HST*. Images in the F336W and F438W filters were acquired using the Ultraviolet-Visible Channel (UVIS) of the Wide Field Camera 3 (WFC3), while the Wide Field Channel (WFC) of the Advanced Camera for Surveys (ACS) was used to acquire the images in the F555W and F814W filters. The list of observations for NGC 339 and NGC 419

is given in Table 1 and Table 2, respectively. These multi-epoch observations provide long temporal baselines for the PM measurements, of 10.75 yr for NGC 339 and 12.67 yr for NGC 419.

The photometric reduction is performed following the prescriptions given in Bellini et al. (2017b), Bellini et al. (2018) and summarised in the following. We analyzed `_flc` images that were also corrected for charge transfer efficiency (CTE, Anderson & Bedin 2010). Briefly, we first performed a single-pass photometry to measure bright stars in each exposure, without subtracting the neighbouring sources. Then, after correcting the instrumental positions for geometric distortions with the solutions provided in Anderson & King (2006), Bellini et al. (2011), we performed a multi-pass photometry with the KS2 program. This simultaneously analyzes all the available images in all the filters, by combining the results of the previous step and also performing neighbour subtraction. Instrumental magnitudes were calibrated into the VEGAMAG photometric system, following the example of Bellini et al. (2017a) and Raso et al. (2020).

The relative PM measurements of NGC 419 used in this work are those determined by Massari et al. (2021). We refer to this paper for the details of the PM measurement procedure, which is based on the techniques developed by Bellini et al. (2014), later improved by Bellini et al. (2018) and Libralato et al. (2018). Briefly, the procedure to measure the relative PMs is iterative. At each step, single-exposure star positions are transformed on to an epoch-matched reference frame (based on the *Gaia* Data Release 2 catalog) by means of a six-parameter linear transformation. Only bright and unsaturated cluster stars are used at this stage. At the first iteration, PMs are assumed to be zero, and cluster members are solely defined based on their position on a CMD. For each star, locally-transformed positions as a function of epoch are linear least-squares fitted. Local transformations help in mitigating small-scale systematic effects. The slope of these fits are direct estimates of the stars PMs. We apply sophisticated data rejection and sigma-clipping at each iteration. Convergence is reached when the predicted difference between the master-frame positions at the reference epoch from one step to the next is negligible. After convergence, spatially variable and colour-dependent systematic effects are corrected as described in Bellini et al. (2014). The relative PMs for NGC 339 were measured following the same procedures.

2.1. Selection criteria

To remove stars that are poorly measured from our catalogues, we applied several photometric and astro-

Program ID	PI	Epoch (yyyy/mm)	Camera	Filter	Exposures $N \times t_{\text{exp}}$
GO-10396	J. Gallagher	2005/11	ACS/WFC	F555W	2×20 s
					4×496 s
				F814W	2×10 s
					4×474 s
GO-14069	N. Bastian	2016/08	WFC3/UVIS	F336W	2×1200 s
					1×700 s
				F438W	1×120 s
					1×180 s
					1×560 s
					1×660 s

Table 1. List of the observations of NGC 339 obtained with *HST* used in this work.

Program ID	PI	Epoch (yyyy/mm)	Camera	Filter	Exposures $N \times t_{\text{exp}}$
GO-10396	J. Gallagher	2006/01	ACS/WFC	F555W	1×20 s
				F814W	2×10 s
					4×474 s
		2006/07	ACS/WFC	F555W	2×20 s
					4×496 s
				F814W	2×10 s
					4×474 s
GO-12257	L. Girardi	2011/08	WFC3/UVIS	F336W	1×400 s
					1×690 s
					2×700 s
					1×740 s
GO-14069	N. Bastian	2016/08	WFC3/UVIS	F438W	1×70 s
					1×150 s
					1×350 s
					1×550 s
GO-15061	N. Bastian	2018/09	WFC3/UVIS	F336W	2×1395 s
					1×3036 s
				F438W	2×1454 s

Table 2. List of the observations of NGC 419 obtained with *HST* used in this work.

metric quality criteria, following the guidelines provided by Libralato et al. (2019). Stars are selected as follows: (i) an iterative 3σ -clipping procedure is applied to the photometric error of all the 4 filters, removing stars with the higher uncertainties: the procedure is stopped after 5 iterations; (ii) the same procedure is applied to PM errors; (iii) we selected stars for which the reduced χ^2 of the PM fit is smaller than two in both PM components; (iv) we applied an iterative 3σ -clipping selection around the mean value of the RADXS^1 parameter; (v) we eliminated sources having a ratio $N_g/N_u < 0.8$, where N_u is the total number of detections for each source and N_g is the number of detections considered of sufficiently good quality by the adopted program. The CMDs of the two clusters resulting from such a selection are shown in Figure 1 and compared with the CMDs built from the complete catalogues. The high quality of the available data allows us to recognize sources 3 – 4 magnitudes below the TO point, even in very crowded regions, which is unfeasible with ground-based observations. It is also possible to clearly identify the different evolutionary sequences, both of the clusters and of the Cloud. Specifically, in NGC 419 we notice the extended main sequence turn off (eMSTO) and two distinct sub giant branches, one of the cluster (the brighter one) and one (the fainter) populated by stars of the SMC (see Massari et al. 2021).

3. CLUSTER MEMBERSHIP

To study the BSS population of these clusters, a crucial step is to remove the contamination from field stars (SMC + Milky Way). To do so, we took advantage of the kinematical measurements. First of all, we considered only bright stars, for which photometric and PM uncertainties are smaller: those with $m_{F555W} < 22.7$ in NGC 339, and those with $m_{F555W} < 22.3$ in NGC 419. The PM distributions of the selected stars are displayed in the vector point diagrams (VPDs; black and red dots in left panels of Figures 2 and 3). To select cluster-members, we thus considered only the stars centered around (0,0) mas yr⁻¹ in the VPD and included within a radius twice the expected total dispersion of cluster members σ . This is computed as the sum in quadrature of two independent terms. The first is the intrinsic velocity dispersion of the cluster, σ_{disp} , while the second is the error associated to the PM measurement, σ_{PM} . Under the assumption of isotropy, the expected dispersion along the two PM com-

¹ A measurement of how much flux there is in the pixels just outside of the core, in excess of the prediction from the PSF; it is positive if the object is broader than the PSF, and negative if it is sharper (Bedin et al. 2008).

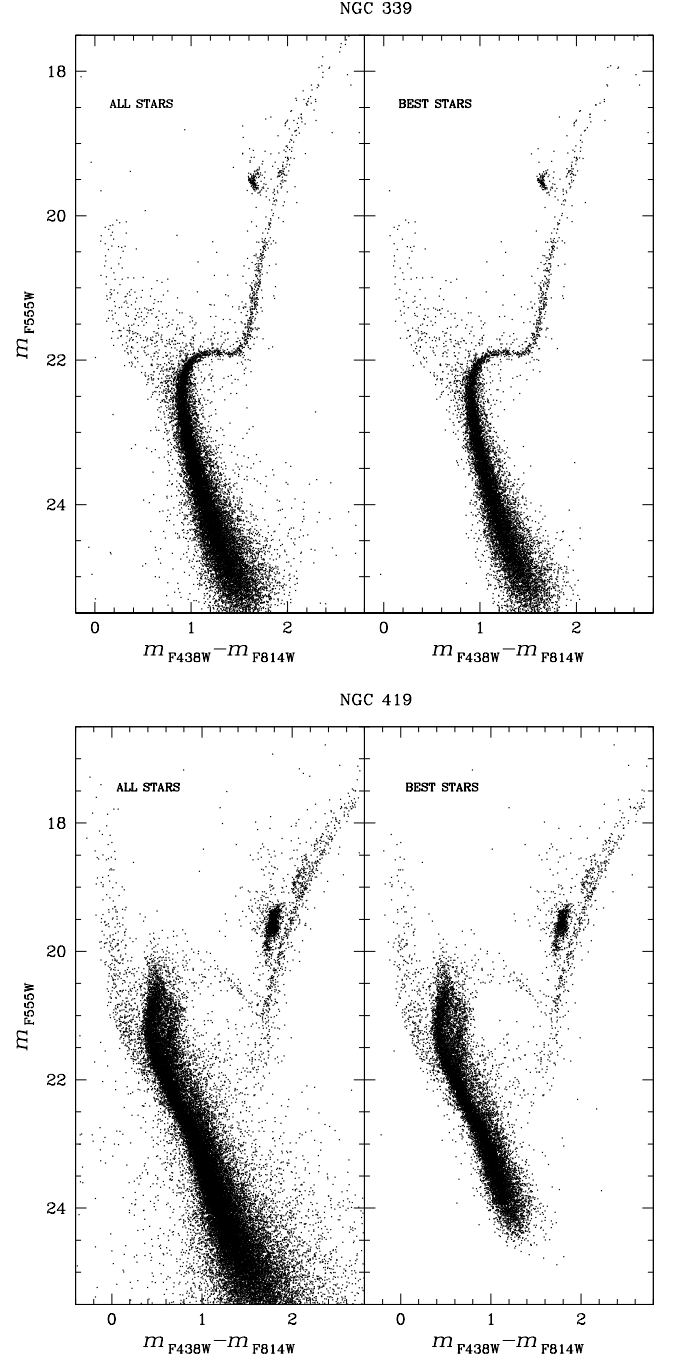


Figure 1. CMDs of NGC 419 (top) and NGC 339 (bottom) built from the catalogues improved by the quality selection discussed in Section 2.1 (right), compared with the complete CMD catalogues (left).

ponents coincide with the dispersion along the line-of-sight, which has been measured to be $\sigma_{\text{los}} = 2.11 \text{ km s}^{-1}$ for NGC 339 (McLaughlin & van der Marel 2005) and $\sigma_{\text{los}} = 2.44 \text{ km s}^{-1}$ for NGC 419 (Song et al. 2019). At the distance of the SMC ($d_{\text{SMC}} \sim 60 \text{ kpc}$, Cioni et al.

2000), these both correspond to $\sim 0.01 \text{ mas yr}^{-1}$. As for the PM uncertainties σ_{PM} , these depend on signal-to noise ratio of each source, hence they vary with the magnitudes. For this reason, we decided to select the average value of the PM error at the faintest magnitude at which the BSS can be detected in a CMD. The σ_{PM} values considered this way are: $\sigma_{\text{PM}} = 0.05 \text{ mas yr}^{-1}$ (at $m_{\text{F555W}} = 22.7$) for NGC 339 and $\sigma_{\text{PM}} = 0.03 \text{ mas yr}^{-1}$ (at $m_{\text{F555W}} = 22.3$) for NGC 419. By adding in quadrature the two terms ($\sigma = \sqrt{\sigma_{\text{los}}^2 + \sigma_{\text{PM}}^2}$) we obtain a total dispersion for the two clusters of $\sigma_{339} = 0.05 \text{ mas yr}^{-1}$ and $\sigma_{419} = 0.03 \text{ mas yr}^{-1}$. The location in the VPD of the likely members so selected is shown in Figures 2 and 3 (red dots). On the CMDs we can see that, thanks to the kinematic selection, we eliminated most of the interlopers located above the MSTO, where BSSs and field stars overlap, thus remarking why the kinematic decontamination is so crucial for our analysis.

A kinematic selection at 3 (instead of 2) σ would have included a larger number of members², at the cost of allowing for a more significant contamination. The adopted 2σ selection ensures the best relative contamination, which we statistically estimated using a Monte Carlo approach. Starting with NGC 339, we first fitted the observed distributions of the two PM components of non-member stars with Gaussian functions. We then randomly generated 1000 such Gaussian distributions by keeping mean, sigma and number of elements fixed, each time counting the number of randomly simulated field stars falling within the selection range of cluster members. The mean relative contamination over these 1000 realisations turned out to be $\sim 5\%$. When only considering stars within one half-mass radius³ (r_h , which is the area within which the analysis of the BSSs will be performed, see Lanzoni et al. 2016, Ferraro et al. 2018), the mean contamination further decreases to $\sim 4\%$. Note that these numbers refer to the global contamination of field stars compared to cluster members. Another useful information is the relative contamination obtained by restricting the analysis to the CMD region where BSSs are located. To estimate this, we selected a sub-sample of field stars with the following criteria: magnitude $m_{\text{F555W}} < 22.7$, color $m_{\text{F438W}} - m_{\text{F814W}} < 0.3$ and distance from the cluster centre $r > r_c = 29''$ (where r_c is the core radius obtained by Glatt et al. 2009). Then, we repeated the Monte Carlo procedure for the PM dis-

tribution of this sub-sample and estimated a residual contamination of 13% for the BSSs within one r_h . As expected, the contamination of the BSSs alone is higher, since the MS of the SMC occupies the same region in the CMD.

The same Monte Carlo technique was adopted to estimate the residual contamination for NGC 419, but with the additional complication given by the fact that this cluster is located along the Magellanic Bridge (Zivick et al. 2019), and is thus contaminated by an additional population of stars that show a different kinematic behaviour from that of the SMC (Massari et al. 2021). To take this complexity into account, we fitted the distributions of the two contaminant populations with distinct Gaussian functions. We then implemented the procedure described above separately for the two distributions. Adding up the contributions of the two populations, we obtained a value for the global residual contamination of 2% within one half-mass radius ($r_h = 36''.73$, derived from r_{hl} , see appendix A) in NGC 419. When limiting the analysis to the BSS region of the CMD, and thus selecting the sample of non-members as the sources with $m_{\text{F555W}} < 22.3$, $m_{\text{F438W}} - m_{\text{F814W}} < 0.4$ and $r > r_c = 12''$ (Glatt et al. 2009) the estimated contamination is $\sim 4\%$. This value is significantly smaller than that obtained for NGC 339, in agreement with our expectations, given the different underlying field population within the SMC field.

4. DYNAMICAL STATE OF THE CLUSTERS

To study the dynamical state of these extra-Galactic clusters, we analyzed the level of segregation of their BSSs. We did so by calculating the $A_{r_h}^+$ parameter, first defined by Alessandrini et al. (2016). In particular, following Lanzoni et al. (2016), we determined the area enclosed between the cumulative radial distributions of BSSs, $\phi_{\text{BSS}}(x)$, and that of a reference (lighter) population, $\phi_{\text{REF}}(x)$, both measured within one half-mass radius:

$$A_{r_h}^+(x) = \int_{x_{\min}}^x (\phi_{\text{BSS}}(x') - \phi_{\text{REF}}(x')) dx' \quad (1)$$

where $x = \log(r/r_h)$ is the cluster-centric distance expressed in logarithmic units, and x_{\min} is the minimum value sampled (usually this coincides with the cluster centre, in which case its value is zero). The value of $A_{r_h}^+$ increases with the level of segregation of the BSSs, effectively tracing the dynamical evolution of the cluster. This has been verified with numerical simulations (Alessandrini et al. 2016) and it has been proven to be effective for a conspicuous sample of old star clusters, both in the Milky Way and in the LMC (see

² Considering a Gaussian distribution, a 3σ selection should include $\sim 99.7\%$ of cluster stars, a 2σ selection only $\sim 95\%$.

³ The value of the half-mass radius is $r_h = 68''.78$ and it was computed from the known value of the projected half-light radius, as described in appendix A.

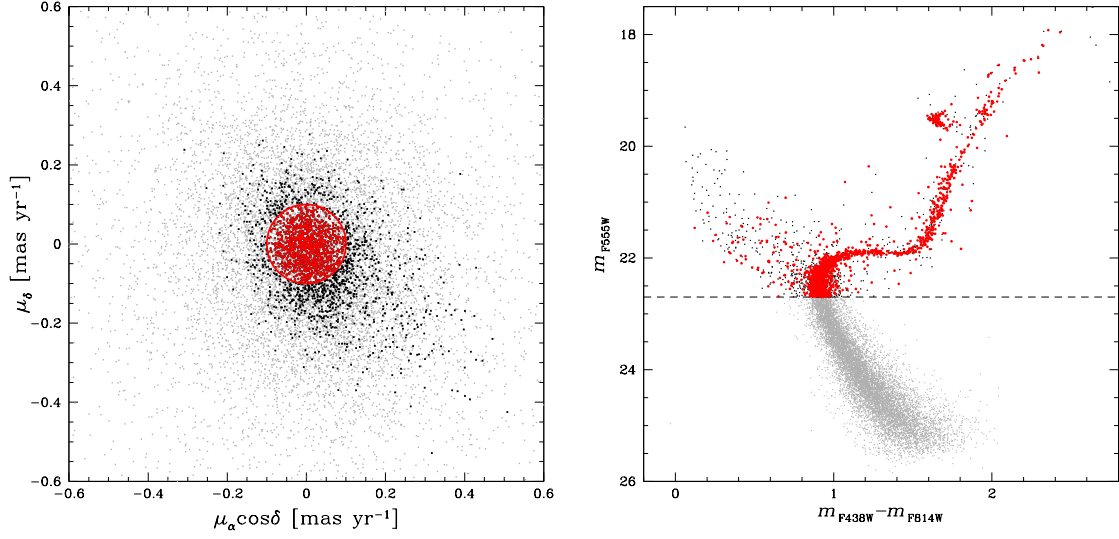


Figure 2. VPD (left) and CMD (right) of NGC 339 for the best stars plotted on the right in Fig. 1. These best stars are plotted here in grey, the stars with $m_{F555W} < 22.7$ are shown as black dots and those selected as cluster members are highlighted in red.

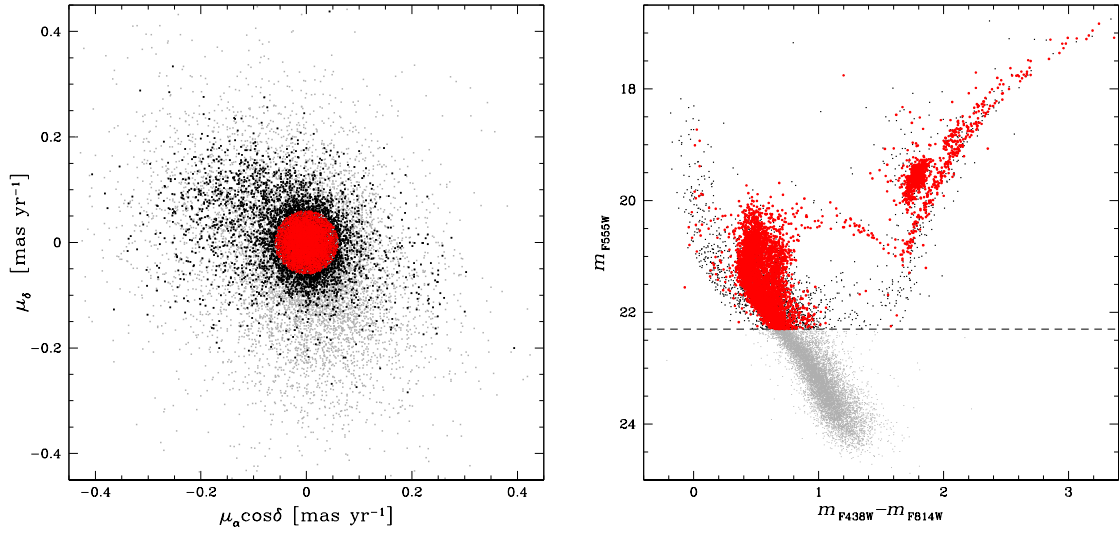


Figure 3. Similar to Figure 2, but for NGC 419.

Ferraro et al. 2018; Ferraro et al. 2019). The value of this parameter is computed within r_h to allow a meaningful comparison among clusters with different structures and sizes.

Practically, to compute the value of A_{rh}^+ we first had to select from the CMD the member BSSs to analyze, along with the reference populations. As shown in Figure 4, we selected three different reference groups, TO stars in green, red giant branch (RGB) stars in cyan and red clump (RC) stars in red, and we estimated the value of A_{rh}^+ for the three cases. We remark at this point that our selection of BSSs is designed to achieve the best purity of the sample, at the cost of completeness. As an example, the BSSs selection was performed in different combinations of filters, and we only retained the stars located in the BSS region in all of these combinations. Moreover, the selection for NGC 419 likely misses the BSSs of the red part of the eMSTO, which are hidden among blue eMSTO stars. Yet, an attempt at recovering them would certainly drain-in contaminating non-BSSs, which we want to avoid.

We built the cumulative radial distribution of BSSs and compared it with each of the reference populations as shown in Figure 5. The value of A_{rh}^+ has been determined for all of the three cases, together with its associated uncertainty. This has been estimated by using a jackknife bootstrapping technique (Lupton 1993). We also performed a Kolmogorov-Smirnov test to determine the level of confidence by which we can consider the two populations as different.

In all cases (see Table 3) we find a value of A_{rh}^+ which is well consistent with zero within 1σ , indicating that the BSSs in NGC 339 have yet to start their segregation, as expected for a dynamically young cluster, based on the evidence gathered from Galactic GCs. Consistently with the measured value of A_{rh}^+ , the results of the KS-test show that the spatial distribution of the BSSs is statistically identical to that of the reference populations.

ref	A_{rh}^+	ε_{A+}	N_{BSS}	N_{ref}
TO	0.04	0.05	31	658
RGB	0.03	0.05	31	341
RC	0.04	0.05	31	76

Table 3. Values of A_{rh}^+ (column 2) and their error ε_{A+} (column 3), computed for the different reference populations (column 1). N_{BSS} and N_{ref} indicate the number of stars considered by the selection of BSSs and of the reference population in NGC 339, respectively.

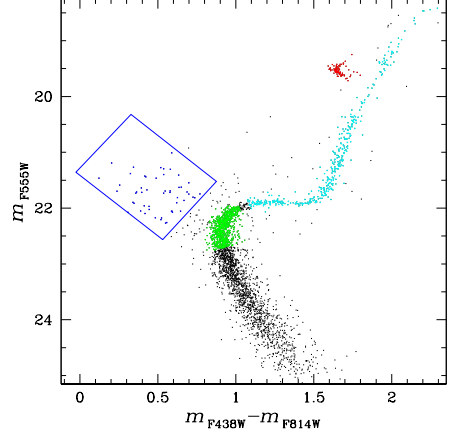


Figure 4. Decontaminated CMD of NGC 339. In blue we selected BSSs, in red, green and cyan the stars belonging to the RC, TO and RGB regions respectively.

The study of the dynamical state of NGC 419 has been performed in the same way, starting from the CMD selection of the stellar populations (Figure 6). The cumulative radial distributions are analyzed out to $r_h = 36''.73$ and are plotted in Figure 7. The values of A_{rh}^+ and the errors computed for this cluster (Table 4) are also consistent with zero within 1σ , meaning that, even in the case of NGC 419, the BSS population is not segregated. This is again confirmed by the results of the KS-test.

ref	A_{rh}^+	ε_{A+}	N_{BSS}	N_{ref}
TO	0.04	0.07	15	1530
RGB	0.00	0.07	15	234
RC	0.00	0.07	15	554

Table 4. Values of A_{rh}^+ (column 2) and their error ε_{A+} (column 3), computed for the different reference populations (column 1). N_{BSS} and N_{ref} indicate the number of stars considered by the selection of BSSs and of the reference population in NGC 419, respectively.

For both clusters, the value of A_{rh}^+ suggests that their BSS populations are not yet centrally segregated. To validate that conclusion is robust, we further performed several checks. First, we tested the effect of residual field contamination on the values of A_{rh}^+ . For NGC 339, for example, the estimated contamination of 13% within r_h implies that 4 out of 31 the identified BSSs are statistically not members. We therefore computed a new value of A_{rh}^+ after randomly removing 4 stars, spatially distributed as field sources (with a uniform spatial distribution), from the BSS distribution. By recomputing

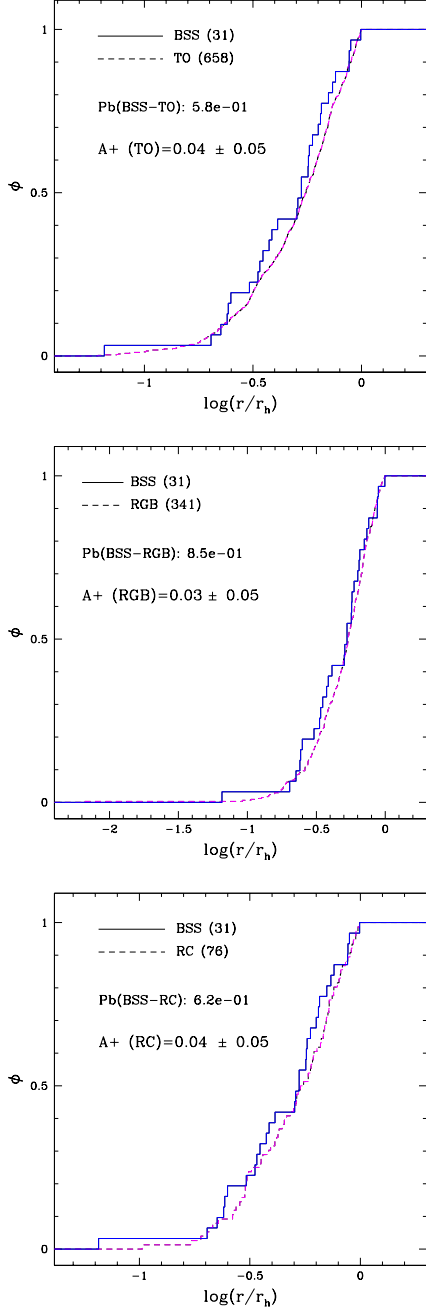


Figure 5. Cumulative radial distributions of BSSs (blue lines) and of the reference stars (magenta lines) in NGC 339. The number of stars in each population is labelled in all panels, together with the corresponding value of A_{rh}^+ and the KS probability that the two samples are drawn from the same parent family.

A_{rh}^+ for this new distributions of 27 BSS and repeating the operation 30 times, we obtained an average value of $A_{rh}^+ \sim 0.05$ (with rms = 0.01), which is perfectly consistent with our original results and thus demonstrates that the effect of the residual contamination is negli-

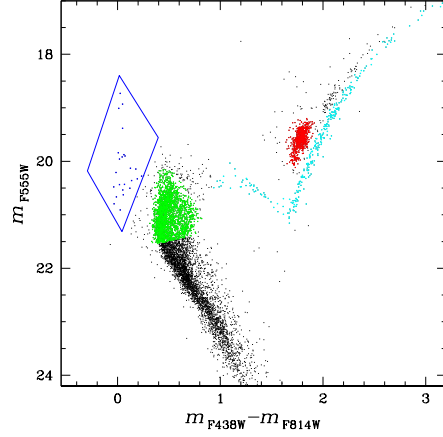


Figure 6. Decontaminated CMD of NGC 419. In blue we selected BSSs, in red, green and cyan the stars belonging to the RC, TO and RGB regions respectively.

ble. We also studied whether the quality selection procedure could influence our final results. To do so we estimated the values of A_{rh}^+ on a catalogue of NGC 339 stars that were not selected based on the quality criteria described in Section 2.1 but only with the 2σ kinematic selection. We obtained the new value $A_{rh}^+ \sim 0.03 \pm 0.04$ that is consistent with the previous values, proving that the technique used to remove low quality sources didn't significantly alter the final result. On the other hand, we noticed a significant difference when the kinematic selection of stellar members is not considered. In fact, we obtained a value of $A_{rh}^+ \sim -0.06 \pm 0.02$, which is not consistent with our previous results and can only be explained as due to the contamination of the BSS sample by a less concentrate population, like SMC stars. This result also proves that the kinematic selection is essential to correctly remove the contamination from the Cloud.

To investigate the connection between the BSS segregation level and the dynamical status of each cluster, we studied the relation between the measured values of A_{rh}^+ and the dynamical/structural properties of the systems. For $\sim 1/3$ of the entire population of Galactic GCs, Ferraro et al. (2018) found a correlation between the value of A_{rh}^+ and the number of current central relaxation times experienced by the systems since formation, as expressed by the parameter $N_{\text{relax}} = t/t_{\text{rc}}$, where t is the cluster age and t_{rc} is its central relaxation time. The value of A_{rh}^+ also shows an anti-correlation with the cluster core radius, in agreement with the fact that dynamically more evolved clusters have smaller r_c and higher levels of segregation. The same relations were also found in old extra-Galactic clusters, situated in the Large Magellanic Cloud (Ferraro et al. 2019).

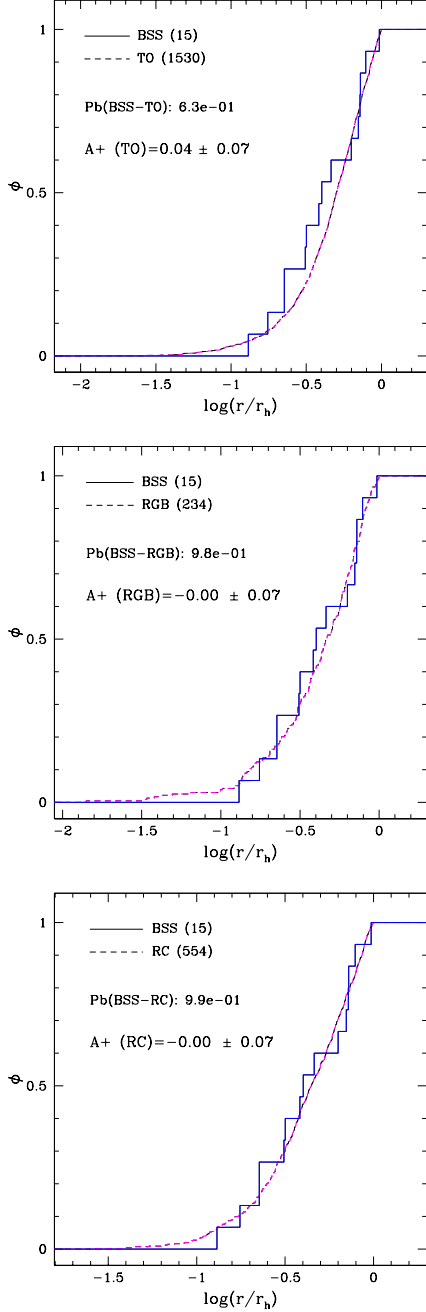


Figure 7. Similar to Figure 5, but for NGC 419.

All the stellar systems that have been studied until now using these techniques, Galactic and extra-Galactic, are chronologically old, while the systems studied in this paper are significantly younger. To verify whether the same relations hold also for these young systems, we determined their central relaxation time t_{rc} , following Djorgovski (1993):

$$t_{rc} = 1.491 \cdot 10^7 \text{ yr} \frac{0.5592}{\ln(0.4 N)} \langle m \rangle^{-1} \rho_{M,0}^{1/2} r_c^3 \quad (2)$$

where N is the estimated total number of stars, $\langle m \rangle$ is the average stellar mass in solar units, $\rho_{M,0}$ is the central mass density in M_\odot/pc^3 and r_c is the core radius in pc. For NGC 339, $\log(\rho_{M,0}) = 1.29$ and $r_c = 7.38$ pc (Mackey & Gilmore 2003), while the average stellar mass ($\langle m \rangle = 0.3M_\odot$) was computed from a synthetic population created by using the evolutionary models presented in Marigo et al. (2008)⁴ and the following physical properties: age $t=6$ Gyr and metallicity $Z=0.001$ (Glatt et al. 2009). The total number of stars (N) has then been derived as the ratio between the total cluster mass ($M \sim 10^5 M_\odot$; Mackey & Gilmore 2003) and $\langle m \rangle$. Once all the parameters were known, we determined the central relaxation time $t_{rc} = 4.16$ Gyr, implying $N_{\text{relax}} = t/t_{rc} = 1.44$. Such a small value of N_{relax} is perfectly consistent with the conclusion derived from the A_{rh}^+ parameter that this cluster is dynamically young. For NGC 419, we determined the average stellar mass in a similar way, obtaining $\langle m \rangle = 0.358M_\odot$ (from $t=1.5$ Gyr, $Z=0.004$, Glatt et al. 2009; $M \sim 0.8 \cdot 10^5 M_\odot$, Song et al. 2019). Not all the parameters needed for the calculation are known and so, to determine the central mass density ($\rho_{M,0}$), we started by estimating the values of the color excess and the distance module. We

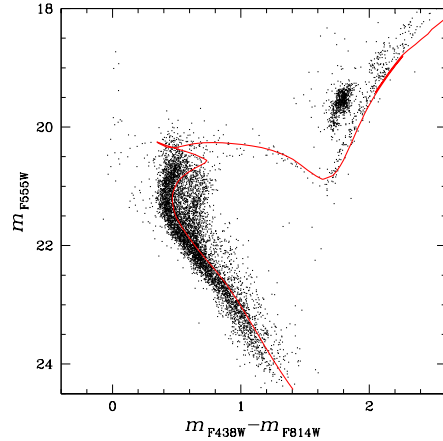


Figure 8. CMD of NGC 419 and the isochrone computed for $t=1.5$ Gyr and $Z=0.004$ (Marigo et al. 2008), superposed as a red line.

fitted by eye the isochrone curve, built with the previous evolutionary models, on the CMD of the cluster (Figure 8), so that it best described the behaviour of all the evolutionary sequences. In this way, we were able to estimate the following values: $E(B - V) = 0.08$ e $(m - M)_0 = 18.94$. By following the prescriptions given

⁴ <http://stev.oapd.inaf.it/cgi-bin/cmd>

in Djorgovski (1993) we computed, with these quantities, the surface brightness in units of luminosity per parsec square (L/pc^2 , eq. 5) and determined the p parameter (eq. 6). With these values, we determined the central luminosity density (eq. 4), from which we obtained the central mass density $\rho_{M,0}$ using the M/L ratio. Finally, we determined the central relaxation time: $t_{\text{rc}} = 1.56$ Gyr, which leads to $N_{\text{relax}} = t/t_{\text{rc}} = 0.962$.

This value of N_{relax} confirms that the system is dynamically young and this theoretical prediction based on the structural properties of the cluster agrees with the results obtained from the observational study of the BSSs.

t	c	r_c	$\mu_{555}(0)$	M_V	M/L
(Gyr)		(arcsec)	(mag arcsec $^{-2}$)	(mag)	($M_{\odot} L_{\odot}^{-1}$)
1.5	1.059	15.22	18.18	-8.85	0.22
(1)	(1)	(1)	(1)	(1)	(2)

Table 5. Parameters of NGC 419. References: Glatt et al. (2009) (1) and Song et al. (2019) (2).

Figures 9 and 10 summarise the main results of our work. In the first plot we present the relation between A_{rh}^+ and the number of relaxations N_{relax} obtained from the study of star clusters in the Milky Way (Ferraro et al. 2018, black symbols) and in the Large Magellanic Cloud (Ferraro et al. 2019, blue symbols). The two SMC clusters analyzed here are positioned along the same sequence in which dynamically young clusters are expected to be located. This means that the study of the dynamical state of clusters based on the radial distribution of BSSs is effective also in this extra-Galactic environment and, especially, it is valid even for clusters that are young or of intermediate age.

The same result is found by studying the trend of A_{rh}^+ as a function of the core radii of the clusters. From the plot in Figure 10, NGC 339 and NGC 419 are located precisely along the sequence of Galactic and LMC clusters, despite being younger and in an extra-Galactic system.

5. CONCLUSIONS

In this paper we analyzed multi-epoch *HST* data of two stellar clusters, NGC 339 and NGC 419 with the aim of determining the stage of the dynamical evolution of these two young systems by using the “dynamical clock” (Ferraro et al. 2012, Lanzoni et al. 2016). In doing this we followed the approach proposed by Lanzoni et al. (2016) and Ferraro et al. (2018) based on the measure

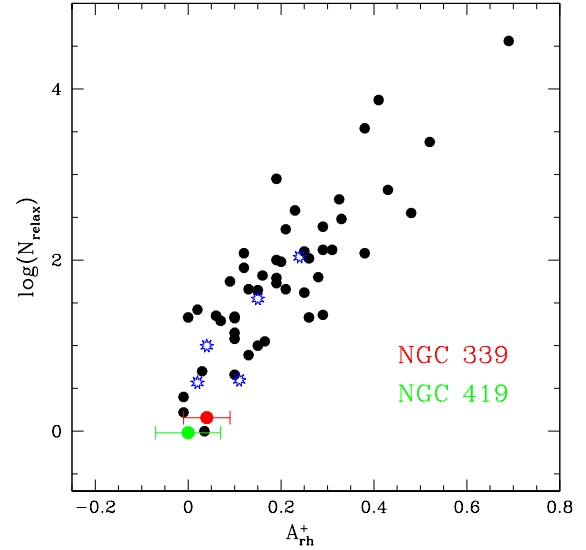


Figure 9. Relation between the number of relaxations $N_{\text{relax}} = t/t_{\text{rc}}$ and the A_{rh}^+ parameter for Galactic clusters (black), for LMC clusters (blue) and for the two systems analyzed in this work.

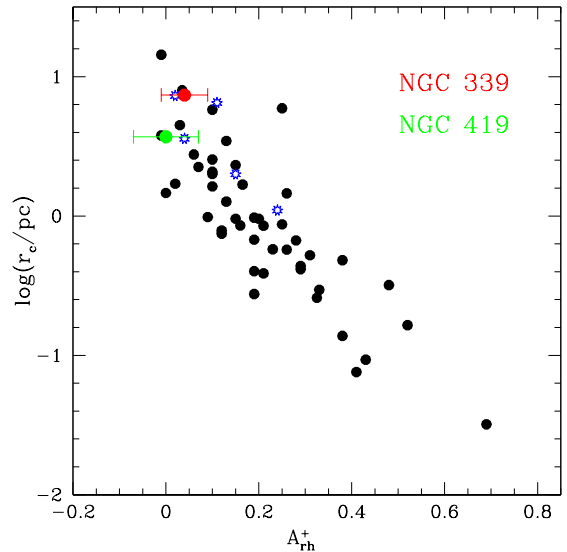


Figure 10. Relation between the core radius r_c and the A_{rh}^+ parameter for star clusters in the MW (black), in the LMC (blue) and the two systems analyzed in this work (red and green circles; see labels).

of the level of segregation of the BSS population via the A_{rh}^+ parameter (see also Alessandrini et al. 2016). After a kinematic selection of Blue Straggler stars and an estimation of their residual contamination, we built cumulative radial distributions of BSSs and of a few reference populations and we found values of A_{rh}^+ consistent with zero for both clusters, indicative of an absence of segre-

gation. By comparing these results with the dynamical properties of the systems (central relaxation times and core radii), we determined that both clusters are dynamically young and that they show the same correlations found in old star clusters from the MW and the LMC, confirming that the A_{rh}^+ parameter is an efficient hand of the “dynamical clock” even for young and intermediate age clusters.

We thank the anonymous referee for comments and suggestions that improved the quality of our paper. This research is part of the project

Cosmic-Lab (“Globular Clusters as Cosmic Laboratories”) at the Physics and Astronomy Department of the Bologna University (see the web page: <http://www.cosmic-lab.eu/Cosmic-Lab/Home.html>). The research is funded by the project Light-on-Dark granted by MIUR through PRIN2017K7REXT contract (PI: Ferraro). This work is also based on observations made with the NASA/ESA Hubble Space Telescope, obtained from the Data Archive at the Space Telescope Science Institute, which is operated by the Association of Universities for Research in Astronomy, Inc., under NASAcontract NAS 5-26555.

APPENDIX

A. THE HALF-MASS RADIUS

The half-mass radius is a three-dimensional parameter and as such it cannot be directly measured from observations. To determine the values of r_h for NGC 339, we used the projected half-light radius $r_{hl} = 52''.10$, measured by Glatt et al. (2011), and we took advantage of the relation existing between this two value when a King model is assumed to be a good representation of the observed density profile. Using a dedicated online software⁵ (Miocchi et al. 2013) we built several King models with different values of the concentration parameter c . For each one of these models the values of r_h and r_{hl} are known, so we can obtain a relation between c and the ratio r_{hl}/r_h . The trend of this relation is shown in Figure 11. For NGC 339, $c=0.755$ (Glatt et al. 2011), so that we had to extrapolate the value $r_{hl}/r_h = 0.757$, that corresponds to a half-mass radius of $r_h = 68''.78$.

For NGC 419, Glatt et al. (2009) determined $r_{hl} = 27''.69$ and $c=1.059$, so we obtained $r_h = 36''.73$.

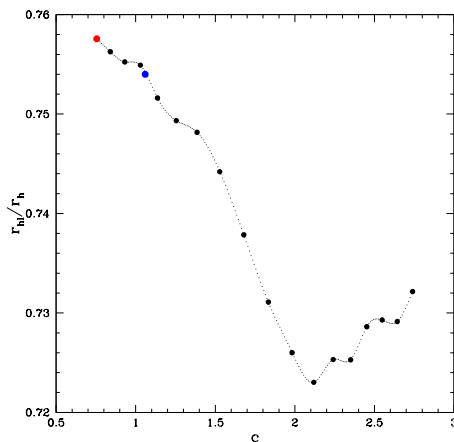


Figure 11. Trend of r_{hl}/r_h with the value of concentration c . The red dot represents the values NGC 339, the blue dot the values for NGC 419.

⁵ <http://www.cosmic-lab.eu/bhking/index.php>

REFERENCES

- Alessandrini, E., Lanzoni, B., Ferraro, F. R., Miocchi, P., & Vesperini, E. 2016, *ApJ*, 833, 252, doi: [10.3847/1538-4357/833/2/252](https://doi.org/10.3847/1538-4357/833/2/252)
- Anderson, J., & Bedin, L. R. 2010, *PASP*, 122, 1035, doi: [10.1086/656399](https://doi.org/10.1086/656399)
- Anderson, J., & King, I. R. 2006, PSFs, Photometry, and Astronomy for the ACS/WFC, Instrument Science Report ACS 2006-01
- Bedin, L. R., King, I. R., Anderson, J., et al. 2008, *ApJ*, 678, 1279, doi: [10.1086/529370](https://doi.org/10.1086/529370)
- Bellini, A., Anderson, J., & Bedin, L. R. 2011, *PASP*, 123, 622, doi: [10.1086/659878](https://doi.org/10.1086/659878)
- Bellini, A., Anderson, J., Bedin, L. R., et al. 2017a, *ApJ*, 842, 6, doi: [10.3847/1538-4357/aa7059](https://doi.org/10.3847/1538-4357/aa7059)
- Bellini, A., Bianchini, P., Varri, A. L., et al. 2017b, *ApJ*, 844, 167, doi: [10.3847/1538-4357/aa7c5f](https://doi.org/10.3847/1538-4357/aa7c5f)
- Bellini, A., Anderson, J., van der Marel, R. P., et al. 2014, *ApJ*, 797, 115, doi: [10.1088/0004-637X/797/2/115](https://doi.org/10.1088/0004-637X/797/2/115)
- Bellini, A., Libralato, M., Bedin, L. R., et al. 2018, *ApJ*, 853, 86, doi: [10.3847/1538-4357/aaa3ec](https://doi.org/10.3847/1538-4357/aaa3ec)
- Cabrera-Ziri, I., Niederhofer, F., Bastian, N., et al. 2016, *MNRAS*, 459, 4218, doi: [10.1093/mnras/stw966](https://doi.org/10.1093/mnras/stw966)
- Cioni, M. R. L., van der Marel, R. P., Loup, C., & Habing, H. J. 2000, *Å*, 359, 601. <https://arxiv.org/abs/astro-ph/0003223>
- Dalessandro, E., Ferraro, F. R., Bastian, N., et al. 2019, *A&A*, 621, A45, doi: [10.1051/0004-6361/201834011](https://doi.org/10.1051/0004-6361/201834011)
- Djorgovski, S. 1993, in *Astronomical Society of the Pacific Conference Series*, Vol. 50, Structure and Dynamics of Globular Clusters, ed. S. G. Djorgovski & G. Meylan, 373
- Ferraro, F. R., Fusi Pecci, F., & Buonanno, R. 1992, *Monthly Notices of the Royal Astronomical Society*, 256, 376, doi: [10.1093/mnras/256.3.376](https://doi.org/10.1093/mnras/256.3.376)
- Ferraro, F. R., Lanzoni, B., Dalessandro, E., et al. 2019, *Nature Astronomy*, 3, 1149, doi: [10.1038/s41550-019-0865-1](https://doi.org/10.1038/s41550-019-0865-1)
- Ferraro, F. R., Pecci, F. F., Cacciari, C., et al. 1993, *AJ*, 106, 2324, doi: [10.1086/116804](https://doi.org/10.1086/116804)
- Ferraro, F. R., Paltrinieri, B., Fusi Pecci, F., et al. 1997, *A&A*, 324, 915. <https://arxiv.org/abs/astro-ph/9703026>
- Ferraro, F. R., Lanzoni, B., Dalessandro, E., et al. 2012, *Nature*, 492, 393, doi: [10.1038/nature11686](https://doi.org/10.1038/nature11686)
- Ferraro, F. R., Lanzoni, B., Raso, S., et al. 2018, *ApJ*, 860, 36, doi: [10.3847/1538-4357/aac01c](https://doi.org/10.3847/1538-4357/aac01c)
- Fiorentino, G., Lanzoni, B., Dalessandro, E., et al. 2014, *ApJ*, 783, 34, doi: [10.1088/0004-637X/783/1/34](https://doi.org/10.1088/0004-637X/783/1/34)
- Glatt, K., Grebel, E. K., Gallagher, John S., I., et al. 2009, *AJ*, 138, 1403, doi: [10.1088/0004-6256/138/5/1403](https://doi.org/10.1088/0004-6256/138/5/1403)
- Glatt, K., Grebel, E. K., Jordi, K., et al. 2011, *AJ*, 142, 36, doi: [10.1088/0004-6256/142/2/36](https://doi.org/10.1088/0004-6256/142/2/36)
- Hills, J. G., & Day, C. A. 1976, *Astrophys. Lett.*, 17, 87
- Lanzoni, B., Ferraro, F. R., Alessandrini, E., et al. 2016, *ApJ*, 833, L29, doi: [10.3847/2041-8213/833/2/L29](https://doi.org/10.3847/2041-8213/833/2/L29)
- Libralato, M., Bellini, A., Piotto, G., et al. 2019, *ApJ*, 873, 109, doi: [10.3847/1538-4357/ab0551](https://doi.org/10.3847/1538-4357/ab0551)
- Libralato, M., Bellini, A., van der Marel, R. P., et al. 2018, *ApJ*, 861, 99, doi: [10.3847/1538-4357/aac6c0](https://doi.org/10.3847/1538-4357/aac6c0)
- Lupton, R. 1993, *Statistics in Theory and Practice* (Princeton, NJ: Princeton Univ. Press)
- Mackey, A. D., & Gilmore, G. F. 2003, *MNRAS*, 338, 120, doi: [10.1046/j.1365-8711.2003.06022.x](https://doi.org/10.1046/j.1365-8711.2003.06022.x)
- Marigo, P., Girardi, L., Bressan, A., et al. 2008, *Å*, 482, 883, doi: [10.1051/0004-6361:20078467](https://doi.org/10.1051/0004-6361:20078467)
- Massari, D., Raso, S., Libralato, M., & Bellini, A. 2021, *MNRAS*, 500, 2012, doi: [10.1093/mnras/staa3497](https://doi.org/10.1093/mnras/staa3497)
- McCrea, W. H. 1964, *MNRAS*, 128, 147, doi: [10.1093/mnras/128.2.147](https://doi.org/10.1093/mnras/128.2.147)
- McLaughlin, D. E., & van der Marel, R. P. 2005, *ApJS*, 161, 304, doi: [10.1086/497429](https://doi.org/10.1086/497429)
- Miocchi, P., Lanzoni, B., Ferraro, F. R., et al. 2013, *ApJ*, 774, 151, doi: [10.1088/0004-637X/774/2/151](https://doi.org/10.1088/0004-637X/774/2/151)
- Raso, S., Pallanca, C., Ferraro, F. R., et al. 2019, *ApJ*, 879, 56, doi: [10.3847/1538-4357/ab2637](https://doi.org/10.3847/1538-4357/ab2637)
- Raso, S., Libralato, M., Bellini, A., et al. 2020, *ApJ*, 895, 15, doi: [10.3847/1538-4357/ab8ae7](https://doi.org/10.3847/1538-4357/ab8ae7)
- Sandage, A. R. 1953, *AJ*, 58, 61, doi: [10.1086/106822](https://doi.org/10.1086/106822)
- Shara, M. M., Saffer, R. A., & Livio, M. 1997, *ApJL*, 489, L59, doi: [10.1086/310952](https://doi.org/10.1086/310952)
- Song, Y.-Y., Mateo, M., Mackey, A. D., et al. 2019, *MNRAS*, 490, 385, doi: [10.1093/mnras/stz2502](https://doi.org/10.1093/mnras/stz2502)
- Zivick, P., Kallivayalil, N., Besla, G., et al. 2019, *ApJ*, 874, 78, doi: [10.3847/1538-4357/ab0554](https://doi.org/10.3847/1538-4357/ab0554)

This figure "orcid-ID.png" is available in "png" format from:

<http://arxiv.org/ps/2202.07677v1>